Lafia Journal of Scientific & Industrial Research (LJSIR), Vol. 3(2), 2025
p-ISSN: 3026 – 9288 e-ISSN: 3027 – 1800 pages: 71 – 78
https://lafiascijournals.org.ng/index.php/ljsir/index ⇒ Published by the Faculty of Science,
Federal University of Lafia, Nasarawa State, Nigeria

Electronic and Optical Properties of Rare Earth Atoms Doped Niobium Dichalcogenides NbX_2 (X=S, Se) Monolayers: A First Principle Study

Godwin Joseph Ibeh[1]*, Jabir Adamu Tahir[1,2] & Alhassan Shuaibu[2]
[1]Department of Physics, Nigerian Defence Academy, Kaduna State, Nigeria
[2]Department of Physics, Kaduna State University, PMB 2339, Kaduna State, Nigeria

Abstract

A First-principles calculation has been carried out to study the electronic, and optical properties of RE (La and Sm) atoms doped monolayer NbX_2 (X=S, Se). The properties are studied through the use of density functional theory (DFT) with Perdew-Burke-Ernzerhof-generalized gradient approximation (PBE-GGA) as exchange correlation functional and Time dependent density functional theory (TDDFT) as implementation in Quantum ESPRESSO code. The electronic band structures, as well as density of states (DOS) of these structures, show both are metallic in nature. The analysis of optical properties reveals that both La and Sm doped NbX_2 (X= S, Se) Monolayer possess maximum absorptivity in the UV range of incident photon's energy with minimum energy loss and decrease in reflectivity. Our complete study about the considered compounds describes them as potential candidates for technological applications in plasmonic and optoelectronic devices.

Keywords: NbX_2 (X= S, Se) Monolayer, density functional theory, dependent density functional theory, electronic and optical properties, rear earth doping

Article History

Submitted
March 23, 2025

Revised
May 19, 2025

First Published Online
July 07, 2025

Correspondences
G. J. Ibeh ✉
gjibeh@nda.edu.ng

doi.org/10.62050/ljsir2025.v3n2.548

Introduction

Lately, there has been growing interest in two-dimensional (2D) transition metal dichalcogenides (TMDCs) because of their distinct properties and potential for electronic and optoelectronic applications [1, 2]. 2D-TMDCs are a type of low-dimensional materials with the formula MX_2, where M represents transition metals such as Nb, Mo, and W, and X denotes S, Se, and Te [3]. However, the properties exhibited by 2D-TMDCs are quite uniform and restricted [4]. To unlock the full potential of 2D-TMDCs in high-performance thin film transistors and to introduce new distinguishing features, effective doping strategies are needed to control their carrier type and adjust the band gap [5]. Typical doping methods for 2D-TMDCs include substitution doping during growth, ion implantation, and surface charge transfer [6]. Yet, in previous doping approaches, ion injection and surface charge transfer in monolayer 2D-TMDC doping often lacked stability, limiting their applications [6, 7]. Substitution doping of 2D-TMDCs has been extensively studied for electronic and optoelectronic applications [7], as well as for room-temperature ferromagnetism [8–10]. Transition elements have been utilized as cationic substitutes for doped 2D-TMDCs, for instance, Nb ion-doped 2D-TMDCs exhibiting p-type transport characteristics and Re ion-doped 2D-TMDCs achieving nearly degenerate n-type doping [11]. Furthermore, recent studies have confirmed ferromagnetism in monolayer MoS2 through in situ Fe-doping at room temperature [10], and enhanced tunable ferromagnetism in V-doped WSe_2 monolayers at 0.5–5 at% V concentrations [9]. Additionally, other transition metal elements have been demonstrated in the in situ substitution of MoS2-doped for electronic applications, such as for Mn [12]. The aforementioned research has shown that the doping of transition metal elements can adjust the electrical, optical, and magnetic properties of 2D-TMDCs [13]. So far, transition metal elements have been widely employed in in situ substitution-doped monolayer 2D-TMDCs. However, the engineering of atomically thin TMDCs by introducing elements with different atomic valences and atomic configurations, such as RE elements, remains challenging. Currently, there are several challenging issues associated with in situ RE element substitution-doped large monolayer 2D-TMDCs.

Rare earth (RE) elements, typically existing as trivalent cations, consist of 15 lanthanides (from lanthanum to lutetium) as well as scandium and yttrium [14]. Previous research has shown that RE ions were frequently incorporated into traditional insulators or semiconductors [15]. RE elements can also serve as effective dopants in TMDC materials. Lanthanide (Ln) ions possess a diverse f-orbit configuration that enables them to absorb and emit photons across the ultraviolet to infrared spectrum through the 4f-4f or 4f-5d transition, making them potential candidates for

enhancing 2D-TMDC semiconductor luminescence [15, 16]. Furthermore, RE dopants with unfilled 4f energy states and charge-transfer state structures may offer robust spin-orbit coupling to adjust the semiconductor properties of the 2D-TMDC's host material [17]. Additionally, first principle calculations have validated the feasibility of incorporating rare earth elements into 2D-TMDCs [18, 19]. Currently, efforts are underway to explore the use of RE element-doped 2D-TMDCs films for optical, electronic, and magnetic applications [20].

Numerous theoretical research studies have explored doping strategies for Niobium dichalcogenides NbX_2 (X=S, Se) to understand their unique electronic and optical properties resulting from their distinct chemical composition and structural phases. These studies have mainly utilized first-principles methods like density functional theory (DFT) to examine the electronic properties and structural stability of NbX_2 (X=S, Se) [21–24]. However, current theoretical works often neglect the complex interactions between chemical composition, structural phase, and the mechanical and optical characteristics of these transition metal dichalcogenides (TMDCs). Additionally, while these studies offer valuable insights into the fundamental properties of NbX2 (X=S, Se), they frequently lack a comprehensive understanding of the multiple phases and symmetries observed in multilayer TMDCs. Furthermore, the existing theoretical models do not thoroughly discuss the doping mechanism between rare earth (RE) elements and them. Therefore, there is a continued need for more comprehensive theoretical investigations that consider the impact of RE doping on the structural, mechanical, electronic, and optical properties of innovative TMDCs. We have presented the structural and mechanical properties of single La and Sm atoms doped NbX2 (X=S, Se) in another work.

In the current study, The Electronic and Optical properties of single La and Sm atoms doped NbX_2 (X=S, Se),based on density functional theory (DFT) and time dependent density functional perturbation theory (TDDFT) has been presented.

Materials and Methods

The first-principles DFT computations were used to derive the theoretical results. Band structure and density of states were determined using the QUANTUM ESPRESSO package [25]. For addressing exchange-correlation, the Perdew-Burke-Ernzerhof (PBE) function form in the generalized gradient approximation (GGA) was employed [26]. Projector-augmented wave (PAW) pseudopotentials were utilized to characterize the interactions of valence and core electrons [27]. A plane-wave kinetic energy cutoff of 50 Ry was set with a charge density of 540Ry [28]. In the self-consistent computation, the energy convergence threshold was fixed at 10^5. The doping was carried out on the $3\times 3\times 1$ super cell of the NbX_2 (X=S, Se) with 27 atoms per unit cell given in Fig. 1, which correspond to 3.7% doping concentration. The model is based on replacing one Nb with Single La and Sm atoms respectively. The atomic coordinates and lattice parameters were optimized using the Broyden-Fletcher-Goldfarb-Shanno (BFGS) algorithm [29] to minimize energy within the numerical approximations. For the electronic DOS and banstructure calculations. The self-consistent convergence accuracy is set at 10^5 eV per atom with the atomic force convergence criteria of 0.03 eV.

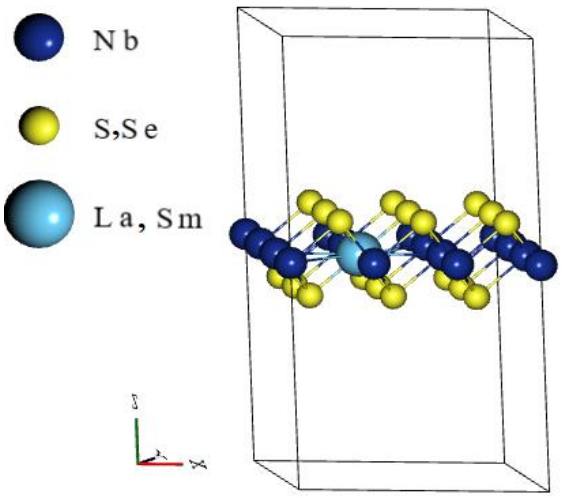

Figure 1: Crystal structure of 3× 3 × 1 supercell of NbX_2 (X= S, Se) Monolayer with DFT-GGA optimized parameters

The optical properties of crystalline materials are mostly calculated using the imaginary $\varepsilon_2(\omega)$ and real $\varepsilon_1(\omega)$ component of the complex dielectric function $\varepsilon(\omega)$ giving by the equation

$$\varepsilon(\omega = \varepsilon_1(\omega) + i\varepsilon_2(\omega) \quad (1)$$

The imaginary part can be calculated from Kubo-Greenwood equation expressed as

$$\varepsilon_2(\omega) = \frac{2\pi e^2}{\Omega\varepsilon_o}\sum_{k,v,c}|\langle\Psi_k^c|u.r|\Psi_k^v\rangle|^2\,\delta(E_k^c - E_k^v - E) \quad (2)$$

Moreover, the real part $\varepsilon_1(\omega)$ of the dielectric function can be determine from the imaginary component using Kramer-Kronig equation given by

$$\varepsilon_1(\omega) = 1 + \left(\frac{2}{\pi}\right)\int_0^\infty d\omega\,\frac{\omega'^2\varepsilon_2(\omega')}{\omega'^2 - \omega^2} \quad (3)$$

$$\alpha(\omega) = \sqrt{2}\omega\left[\sqrt{\{\varepsilon_1(\omega)\}^2 + \{\varepsilon_2(\omega)\}^2} - \varepsilon_1(\omega)\right]^{\frac{1}{2}} \quad (4)$$

$$\sigma(\omega) = \frac{\omega\varepsilon_2(\omega)}{4\pi} \quad (5)$$

$$n = \sqrt{\left(\frac{\sqrt{\{\varepsilon_1(\omega)\}^2+\{\varepsilon_2(\omega)\}^2}+\varepsilon_1(\omega)}{2}\right)} \quad (6)$$

In the above equation ω is the frequency of phonon, Ω is the unit cell volume, u is the unit vector, e is the charge of electron also Ψ_k^c and Ψ_k^v are wavefunction for conduction and valence band electrons respectively at k. $\alpha(\omega)$ is the absorption coefficient, $\sigma(\omega)$ optical conductivity and n the refractive index of the material.

Results and Discussion

Electronic properties of La and Sm doped monolayer NbS_2

Figure 2(a & b) shows our calculated band structures of La and Sm-doped NbS_2 monolayer within a high symmetry brillioun zone, from which one can see an asymmetry in the La doped is more close to the valance band within (0 to 4eV) Fig. 2(a) while Sm doped moved the Fermi level close to the valance band within (0 to -4eV) Fig. (2(b)). Showing that both the monolayers display a strong metallic character. It is noteworthy that the number of electronic bands around E_F is increased significantly when compare to that in pristine monolayers of these compounds. Furthermore, the possible band gap in conduction band in the monolayer disappeared after doping due to the La(Sm) 5d(4f) states, which changes the electronic property of $NbSe_2$ monolayers.

The calculated DOS of the upon doping of NbS_2 monolayer by La element displays a distinct regions and confirmed the metallic behavior as shown in the band structure, while the Fermi level is located between at a high peak having the number of states approximately at 9.2 states/eV (as seen Fig. 2(c)). The lower valence band (- 6.7 to -5.2 eV) results from S 4s orbital with a less contribution of both Nb-d and La-d character. The subsequent region (- 2.8 to 2.6 eV) makes through the mixed of La-d and S-p states in addition Nb-d orbital is dominated in this energy span. The conduction bands (0 to 4 eV) are derived from mixed Nb-4d and S p-states with a less contribution of La-d character.

The Total DOS curve for Sm-doped monolayer NbS_2 (Fig. 2(d)) exhibits a strong metallic character. It is evidently noticed that the Fermi level is lying at a high peak with an N (EF) value around 7.8 states/eV, while the DOS is also divided into some distinct regions. The lower valence band (-1.5 to 0) is originated from S 4s-orbital, with a less contribution of Nb-4d and Sm 4f character. The next region (-2. to2.5) results from a mixed of Nb-d and S-p states with a few contribution of Sm 5f-state. The subsequent bands (-2 to 1) develop the assistance of S 4p-state. The conduction bands (1.5 to 4 eV) are composed of hybridized Nb-d and S-p-states with a small contribution of Sm-4f character.

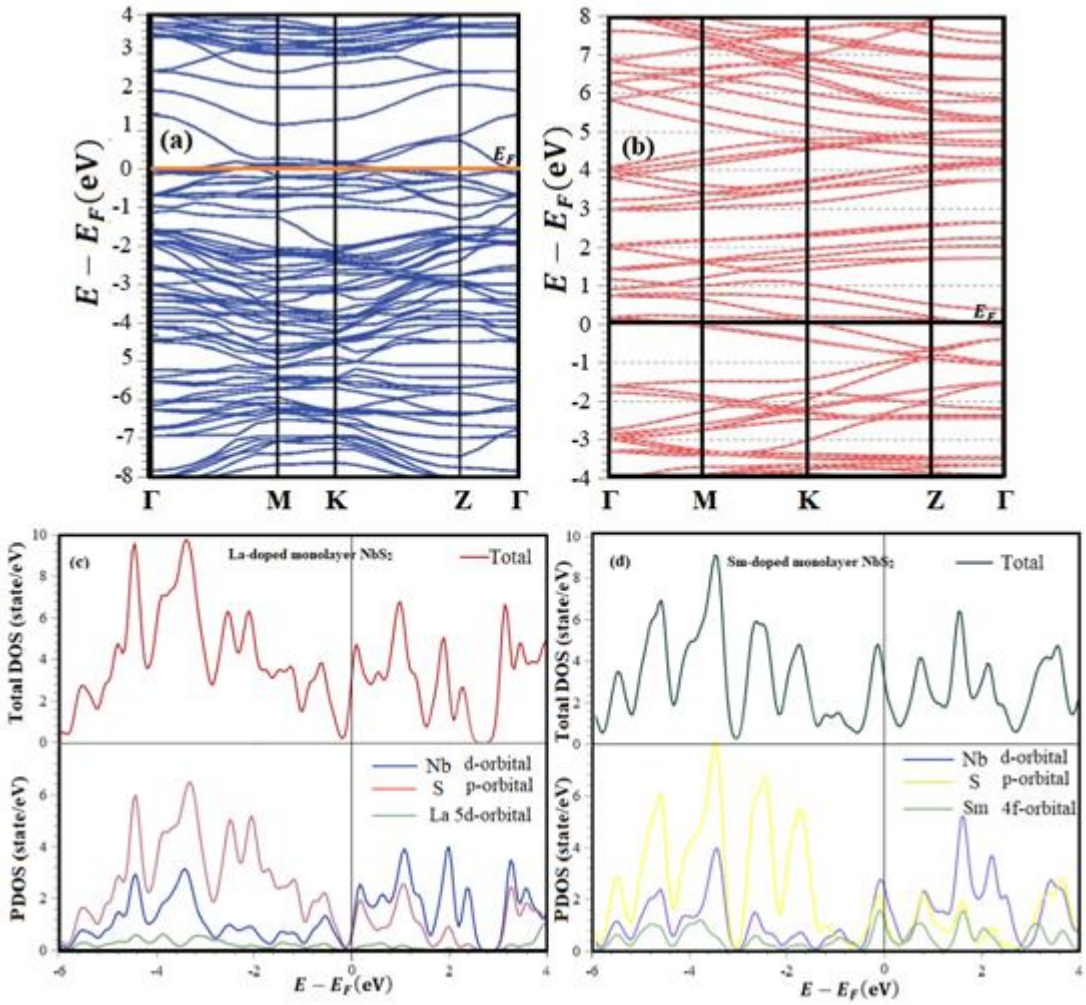

Figure 2: Calculated electronic band structure, DOS and PDOS of state of La and Sm doped NbS_2 monolayer using DFT-GGA optimized parameters

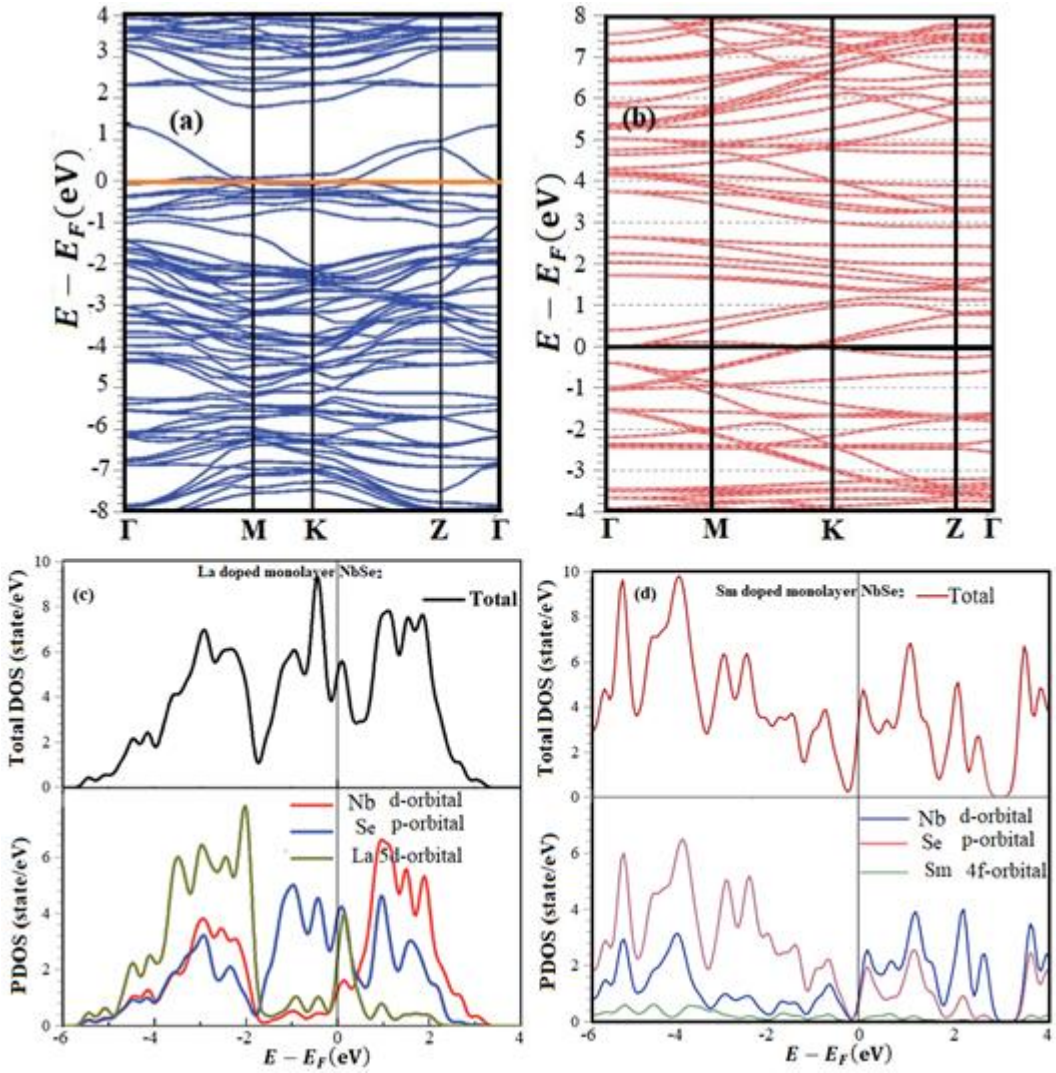

Figure 3: Calculated electronic band structure, DOS and PDOS of state of La and Sm doped $NbSe_2$ Monolayer using DFT-GGA optimized parameters

Electronic properties of La and Sm doped monolayer $NbSe_2$

Upon doping $NbSe_2$ monolayer by Laand Sm atomsthe calculated band structures given in Fig. 3(a & b), the band structures shows similar character in case of doping NbS_2 monolayer while for the DOS of La doped $NbSe_2$ monolayer Fig. 3(c) we observed that Fermi level is crossing a high peak, and its corresponding number of state is about 8.3 states/eV. The lower valence band (−1.7 to 0) is originated from Se 4o-character, with a small contribution of Nb-4d character. The subsequent region (−2.9 to −3.7) results from La 4d state with a few contribution of Se 4p-state. The next bands (−2.1 to 1.2) are derived from a combination of Nb-4d and Se 4p-state with a less contribution of La-5d orbital around Fermi level. The conduction bands (2.1 to 4 eV) are derived from a combination of Nb-5d, Se-4p and La-4d orbitals states.

In Fig. 3(d), a high DOS peak is centered on the Fermi level with 5.7 states/eV. The lower valence band located at − 2 eV to − 0 eV is composed by Se-4 s and Nb4d states, and it is dominated by a Se-4 s state. The middle valence states centered from −3.0 eV up to 0.3.2 eV originates through Se-4p, Nb-4d and Sm-4f states where Se-4p and Nb-4d states are dominant. The electronic bands located from –1.2 eV to 1.1 eV are made up of Nb-4d, and Se-4p states with a few contributions of Sm-5d states. The conduction states spanning between 2.0 and 4 eV consists of Nb-4d s, Se-4p and Sm-4f states where Se-4p states are dominant.

Effect of single La and Sm atoms doped on optical properties of NbX_2 (X=S, Se) monolayers

For the effect of La and Sm doped on the optical properties of $NbSX_2$ (X=S, Se) we consider only the polarization along z-axis which is corresponding to the (0 0 1) plane during the construction of the super cell, Hence Fig. 4 (a–f) gives the obtained results for optical absorption, optical conductivity and Reflectivity while Fig. 4(a & b) gives the obtained results of loss function for both La and Sm doped $NbSX_2$ (X=S, Se) monolayers.

From Fig. 4(a & b), it is noticeable that the strong absorption peak occurs for both La and Sm atoms doped in the $NbSX_2$ (X=S, Se) monolayers., and is centered at higher photon energies of 91 $x10^4$ and 86

$x10^4$ cm^{-1} for $NbSe_2$ monolayer and 81 $x10^4$ and 86 $x10^4$ cm^{-1} for NbS_2 monolayer respectively. When considering the corresponding photon energy values that fluctuate between the intervals, the first span displays the tiny optical absorption property of 0 to 2.4 eV, and 0 to 2.6 eV, for La and Sm atoms doped in both NbS_2 and $NbSe_2$ monolayers, respectively. The maximum absorption coefficient at moderate electromagnetic energy radiation is shown in the second spectral window between (2.2–5.8 eV), and (2.4–6.9 eV) for both La and Sm doped NbS_2 and $NbSe_2$ monolayers, respectively. An optical absorption has been recorded for photon energy levels between (6.9 to 8.2 eV), and (8.1 to 8.9 eV), while there is an increase in optical absorption around (9.8 to 12.8 eV), and (9.88 to 12.88 eV) for these doped systems, respectively. Following that, we observed a discernible drop in coefficient absorption about (12.8 to 34 eV), and (13.1 to 34 eV) for the whole doped systems. Remarkably, a structural shoulder results at photon energy values of 35.6, 36 eV for both La and Sm doped systems respectively.

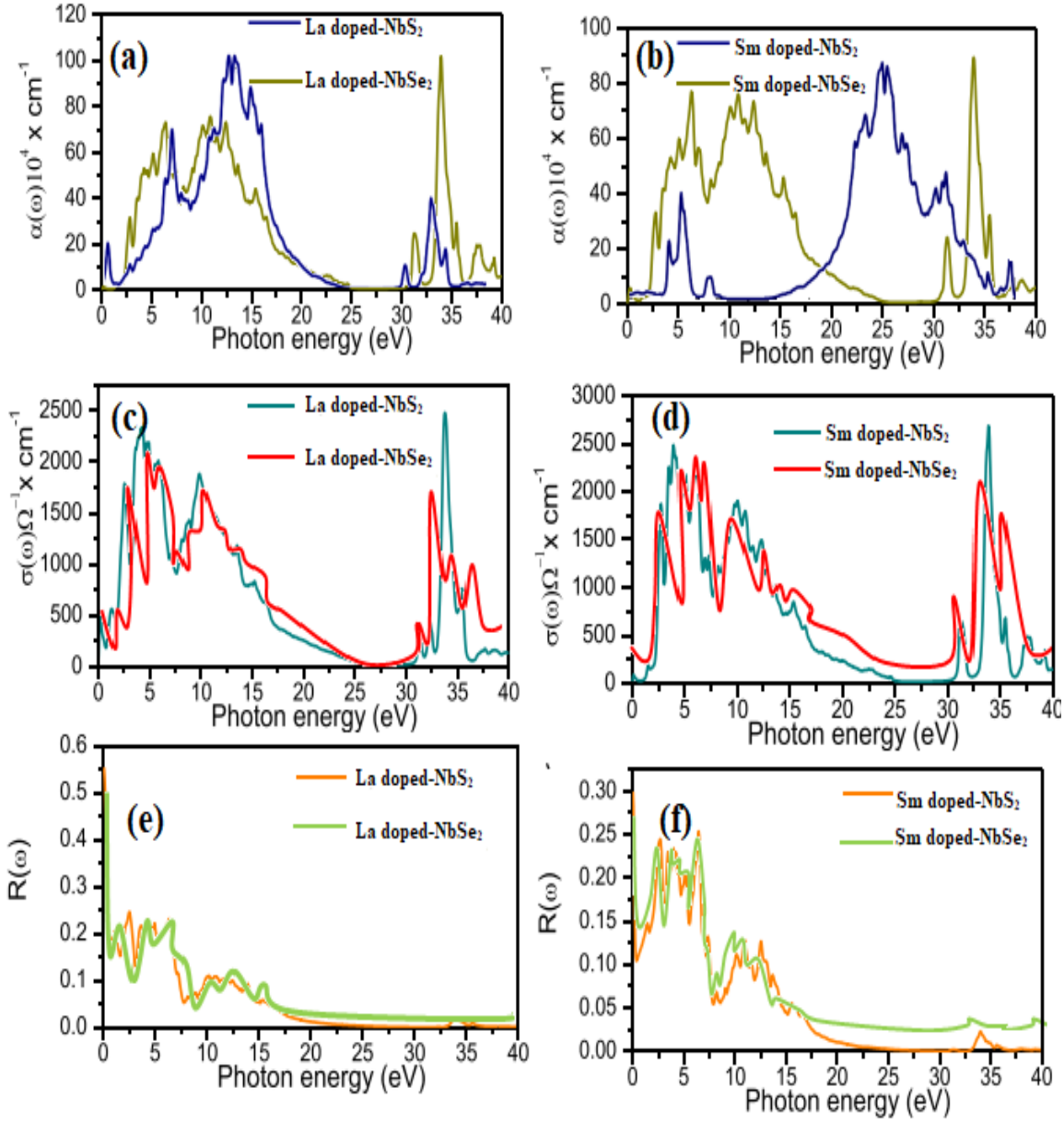

Figure 4: Calculated optical properties (optical absorption, optical conductivity and reflectivity) of La and Sm doped NbX_2 (X=S, Se) Monolayer

The calculated optical conductivity of La and Sm atoms doped NbS_2 and $NbSe_2$ monolayers are shown in Fig. 4(c & d) respectively, although the optical conductivity's descending infrared (IR) spectral spans always exhibit a metallic quality in both bulk and pristine monolayers of these materials. However, upon doping the monolayers with these Rear earth (La and Sm) elements, the optical conductivity also reveals a metallic state in these doped systems, as shown in (Fig. 4(c & d)). Observably, the optical conductivity fits the

basic Drude model much clearly than that of pristine monolayers. Keeping in mind that a broad peak occurs at increasing photon energy and that the development of Drude peaks in the mid-infrared (mid-IR) region is a good indicator of metallic conduction. It appears that σ (ω) grows in electromagnetic radiation with wavelengths ranging from 2.6 to 10.8 eV, while σ (ω) decreases in photon energy within the 12.6–26 eV range. Furthermore, the optical conductivity vanishes in the electromagnetic energy radiation ranging from 26 to 32 eV. The obtained highest value of the conductivity are 2660, and 2600 Ω^{-1} cm^{-1} at phonon energy ranges of 34.6 and 36.4 eV for with La, and SmdopedNb$S_2$and NbSe_2monolayer. These spectra have several maxima and minima at some distinctive energy regimes. Furthermore, the optical conductivity of these 2D materials increases as a result of absorbing photons. For comparison, the recent theoretical calculation of the optical conductivity of NbSX_2 (X=S, Se) monolayers exhibited a metallic behavior, described by a zero-photon energy spectral peak that reduces with decaying temperature. Numerous inter-band transitions were detected in the range 10000–40000 cm^{-1} [22–24]. It was inferred that the absolute values of σ (ω) were normally an order of magnitude greater in the region ω = 0.

Reflectivity is a prominent concept to illustrate the optical nature of solids. Then, the response to the linear optical behavior is characterized through the normal incident reflectivity R (ω) transitions between the valence bands and the downward conduction bands. . Interestingly, upon the doping with the Rear earth atoms (Sm, and La) elements, the reflectivity becomes as higher as in the energy range of 0 to 0.7 eV because these 2D materials own a metallic nature. In addition, moderate prominent peaks are detectable in the range of visible-ultraviolet light (1.5 to 7.4 eV), (2.5 to 7.2 eV), for La, Sm, atoms, respectively doped in NbSe_2monolayer. A reduced reflectivity was achieved in the ultraviolet regime (7.5 to 20 eV) for all two-dimensional materials under study (Fig. 4(e & f)). Hence, the reflectivity is recorded to be approximately zero at the photon energy interval of 21 to 40 eV, whilst an augmentation in the reflectivity is attained in the energy regime 0 to 0.7 eV for all the systems under research. Note that the maximum reflectivity value of about 0.55, 0.30, occurs between the energy spans of 0 to 0.5 eV for La and Sm atoms doped NbSe_2 monolayer. Also, the value drops in the high energy region with some structural peaks as an outcome of intra-band transition. Interestingly, the intra-band transitions mainly occur from chalcogen Se p bands to the Nb d band. The considerable reflectivity for energy less than 1 eV designates the feature of high conductance in the lesser energy span. On the basis of Drude type analysis, the NbSe_2 monolayer shows metallic nature without the involvement of excitons, however, spectra are approximately similar to that for MoS_2. This similarity is evident from the ultra-violet and vacuum ultra-violet region [21, 23].

Conclusion

Conclusively, we systematically studied the electronic and optical properties of single La and Sm atoms doped NbX_2 (X=S, Se) monolayer within DFT and TDDFPT as implemented in QE. The obtained results for the electronic properties shows that both La and Sm atoms doped NbX_2(X=S, Se) monolayers are metallic in nature. For the optical properties investigations it was observed that the highest obtained value of the conductivity are 2660, and 2600 Ω^{-1} cm^{-1} at phonon energy ranges of 34.6, and 36.4 eV for with La, and Sm doped NbS_2 and NbSe_2 monolayer respectively.This is an excellent ultraviolet (UV) range of incident photon's energy for the 2D TMDS. Despite that there's lack of experimental results to affirmed these, but we may probably conclude that the studiedcan serve as potential candidates for technological applications in plasmonic and optoelectronic devices.

Conflict of interest: There is no conflict of interest.

Acknowledgements: We thank and appreciate the gesture of staff in charge of Computational Physics Lab. of the Department of Physics, Kaduna State University for allowing us to carry out all our calculation with High precision computers.

References

[1] Wang, Q. H., Kalantar-Zadeh, K., Kis, A., Coleman, J. N. & Strano, M. S. (2012). Electronics and optoelectronics of two-dimensional transition metal dichalcogenides. *Nat. Nanotechn.*, 7, 699–712. https://doi.org/10.1038/nnano.2010.2

[2] Zhang, K., Feng, S., Wang, J., Azcatl, A., Lu, N., Addou, R., Wang, N., Zhou, C., Lerach, J., Bojan, V., *et al*. (2015). Manganese doping of monolayer MoS_2: The substrate is critical. *Nano Lett.*, 15, 6586–6591. https://doi.org/10.1021/acs.nanolett.5b05063

[3] Wang, Y., Tseng, L.-T., Murmu, P. P., Bao, N., Kennedy, J., Ionesc, M., Ding, J., Suzuki, K., Li, S. & Yi, J. (2017). Defects engineering induced room temperature ferromagnetism in transition metal doped MoS_2. *Mater. Des.*, 121, 77–84. https://doi.org/10.1016/j.matdes.2017.02.034

[4] Li, W., Huang, J., Han, B., Xie, C., Huang, X., Tian, K., Zeng, Y., Zhao, Z., Gao, P., Zhang, Y., *et al*. (2020). Molten-salt-assisted chemical vapor deposition process for substitutional doping of monolayer MoS_2 and effectively altering the electronic structure and phononic properties. *Adv. Sci.*, 7, 2001080. https://doi.org/10.1002/advs.202001080

[5] Tang, J., Wei, Z., Wang, Q., Wang, Y., Han, B., Li, X., Huang, B., Liao, M., Liu, J., Li, N., *et al*. (2020). In situ oxygen doping of monolayer MoS_2 for novel electronics. *Small.*, 16, 2004276. https://doi.org/10.1002/smll.202004276

[6] Zhao, Y., Xu, K., Pan, F., Zhou, C., Zhou, F. & Chai, Y. (2017). Doping, contact and interface engineering of two-dimensional layered transition metal dichalcogenides transistors. *Adv. Funct. Mater.*, 27, 1603484. https://doi.org/10.1002/adfm.201603484

[7] Qin, Z., Loh, L., Wang, J., Xu, X., Zhang, Q., Haas, B., Alvarez, C., Okuno, H., Yong, J. Z., Schultz, T., *et al*. (2019). Growth of Nb-doped monolayer WS_2 by liquid-phase precursor mixing. *ACS Nano*, 13, 10768–10775. https://doi.org/10.1021/acsnano.9b05574

[8] Zhang, F., Zheng, B., Sebastian, A., Olson, D. H., Liu, M., Fujisawa, K., Pham, Y. T. H., Jimenez, V. O., Kalappattil, V., Miao, L., *et al*. (2020). Monolayer vanadium-doped tungsten disulfide: A room-temperature dilute magnetic semiconductor. *Adv. Sci.*, 7, 2001174. https://doi.org/10.1002/advs.202001174

[9] Pham, Y. T. H., Liu, M., Jimenez, V. O., Yu, Z., Kalappattil, V., Zhang, F., Wang, K., Williams, T., Terrones, M. & Phan, M. H. (2020). Tunable ferromagnetism and thermally induced spin flip in vanadium-doped tungsten diselenide monolayers at room temperature. *Adv. Mater.*, 32, 2003607. https://doi.org/10.1002/adma.202003607

[10] Fu, S., Kang, K., Shayan, K., Yoshimura, A., Dadras, S., Wang, X., Zhang, L., Chen, S., Liu, N., Jindal, A., *et al*. (2020). Enabling room temperature ferromagnetism in monolayer MoS_2 via in situ iron-doping. *Nat. Commun.* 11, 2034. https://doi.org/10.1038/s41467-020-15877-7

[11] Zhang, K., Bersch, B. M., Joshi, J., Addou, R., Cormier, C. R., Zhang, C., Xu, K., Briggs, N. C., Wang, K., Subramanian, S., *et al*. (2018). Tuning the electronic and photonic properties of monolayer MoS_2 via in situ rhenium substitutional doping. *Adv. Funct. Mater.* 28, 1706950. https://doi.org/10.1002/adfm.201706950

[12] Cai, Z., Shen, T., Zhu, Q., Feng, S., Yu, Q., Liu, J., Tang, L., Zhao, Y., Wang, J., Liu, B., *et al*. (2020). Dual-additive assisted chemical vapor deposition for the growth of Mn-doped 2D MoS_2 with tunable electronic properties. *Small* , 16, 1903181. https://doi.org/10.1002/smll.201903181

[13] Feng, S., Lin, Z., Gan, X., Lv, R. & Terrones, M. (2017). Doping two-dimensional materials: Ultra-sensitive sensors, band gap tuning and ferromagnetic monolayers. *Nanoscale Horiz.*, 2, 72–80. https://doi.org/10.1039/C6NH00192K

[14] Qin, X., Liu, X., Huang, W., Bettinelli, M. & Liu, X. (2017). Lanthanide-activated phosphors based on 4f-5d optical transitions: Theoretical and experimental aspects. *Chem. Rev.*, 117, 4488–4527. https://doi.org/10.1021/acs.chemrev.6b00691

[15] Gai, S., Li, C., Yang, P. & Lin, J. (2014). Recent progress in rare earth micro/nanocrystals: Soft chemical synthesis, luminescent properties, and biomedical applications. *Chem. Rev.*, 114, 2343–2389. https://doi.org/10.1021/cr4001594

[16] Bai, G., Yuan, S., Zhao, Y., Yang, Z., Choi, S. Y., Chai, Y., Yu, S. F., Lau, S. P. & Hao, J. (2016). 2D layered materials of rare-earth Er-doped MoS_2 with NIR-to-NIR down- and up-conversion photoluminescence. *Adv. Mater.*, 28, 7472–7477.

[17] Zhao, Q., Lu, Q., Liu, Y. & Zhang, M. (2019). Two-dimensional Dy doped MoS_2 ferromagnetic sheets. *Appl. Surf. Sci.* 471, 118–123. https://doi.org/10.1016/j.apsusc.2018.12.100/

[18] Ouma, C. N. M., Singh, S., Obodo, K. O., Amolo, G. O. & Romero, A. H. (2017). Controlling the magnetic and optical responses of a MoS_2 monolayer by lanthanide substitutional doping: A first-principles study. *Phys. Chem. Chem. Phys.*, 19, 25555–25563. https://doi.org/10.1039/C7CP03160B

[19] Majid, A., Imtiaz, A. & Yoshiya, M. (2016). A density functional theory study of electronic and magnetic properties of rare earth doped monolayered molybdenum disulphide. *J. Appl. Phys.*, 120, 142124. https://doi.org/10.1063/1.4963380/

[20] Zhang, Z., Zhao, H., Zhang, C., Luo, F. & Du, Y. (2020). Rare-earth-incorporated low-dimensional chalcogenides: Dry-method syntheses and applications. *InfoMat* 2, 466–482. https://doi.org/10.1002/inf2.12083/

[21] Ni, JunJie, Lu Yang, & TianYun Wang (2024). Effect of transition metal doping on the photoelectric structure of single layer NbS2 under defects. *Modern Physics Letters B*, 38(04), 2350222. https://doi.org/10.1142/S0217984923502226/

[22] Tang, M., Zhao, P., Wang, L., Zhu, L., Wu, Z. & Zhang, D. (2023). Density functional theory study of adsorption of dissolved gas in transformer oil on a metal (Ag, Pd, and Pt)-doped $NbSe_2$ monolayer ACS. *Appl. Nano Mater.*, 6, 5517-5526. https://pubs.acs.org/doi/10.1021/acsanm.3c00017/

[23] Lv, X., Wei, W., Sun, Q., Huang, B. & Dai, Y. (2017). A first-principles study of $NbSe_2$ monolayer as anode materials for rechargeable lithium-ion and sodium-ion batteries. *J. Phys. D. Appl. Phys.*, 50, 235501. https://doi.org/10.1088/1361-6463/aca4de

[24] Ni, Junjie, Lu Yang, & Shu Chen. (2024). Effect of transition metal doping on the photoelectric effect of monolayer NbS2 under strain: First-principles calculations. *Modern Physics Letters B*, 38(04), 2450001.

[25] Giannozzi, P., Baroni, S., Bonini, N., Calandra, M., Car, R., Cavazzoni, C., Ceresoli, D., Chiarotti, G. L., Cococcioni, M., Dabo, I., Dal Corso, A., de Gironcoli, S., Fabris, S., Fratesi, G., Gebauer, R., Gerstmann, U., Gougoussis, C., Kokalj, A., Lazzeri, M., MartinSamos, L., Marzari, N., Mauri, F., Mazzarello, R., Paolini, S., Pasquarello, A., Paulatto, L., Sbraccia, C., Scandolo, S., Sclauzero, G., Seitsonen, A. P., Smogunov, A., Umari, P. & Wentzcovitch, R. M. (2009). Quantum Espresso: A modular and open-source software project for quantum simulations of materials. *J. Phys. Condens. Matter*, 21, 395502.

[26] Perdew J. P., Burke, K. & Ernzerhof, M. (1996). Generalized gradient approximation made simple Phys. Rev. Lett., 77, 3865-3868.

[27] Solanki, M. B., Shinde, S. & Parekh, B. B. (2022). First-principles calculation of the electronic structure, elastic and optical properties of $LiSn_2N_3$ nitrogen base stable perovskite semiconductor material. *Mater. Today Proc*., 67, 943-947

[28] Bartolotti, L. J. & Flurchick, K. (1996). An introduction to density functional theory. *Rev. Comput. Chem*., 187-216.

[29] Oumertem, M., Maouche, D., Berri, S., N., Rai, D. P., Khenata, R. & Ibrir, M. (2019). Theoretical investigation of the structural, electronic and thermodynamic properties of cubic and orthorhombic $XZrS_3$ (X = Ba, Sr, Ca) compounds. *J. Comput. Electron*., 18, 415-427.

Citing this Article

Ibeh, G. J., Tahir, J. A. & Shuaibu, A. (2025). Electronic and optical properties of rare earth atoms doped niobium dichalcogenides NbX_2 (X=S, Se) monolayers: A first principle study. *Lafia Journal of Scientific and Industrial Research, 3*(2), 71 – 78. https://doi.org/10.62050/ljsir2025.v3n2.548